Indication of a Very Large Proton Diffusion in Ice I_h. III. Fluorescence Quenching of 1-Naphthol Derivatives

Anna Uritski, Itay Presiado, and Dan Huppert*

Raymond and Beverly Sackler Faculty of Exact Sciences, School of Chemistry, Tel Aviv University, Tel Aviv 69978, Israel

Received: July 15, 2008; Revised Manuscript Received: December 7, 2008

The effects of excess protons on the fluorescence quenching process of 1-naphthol-4-sulfonate (1N4S) and 1-naphthol-3-sulfonate (1N3S) in methanol-doped ice samples were studied by employing a time-resolved emission technique. We found that the fluorescence quenching of the deprotonated form RO^-* of both photoacids by protonation is very efficient in ice, whereas in liquid water the proton fluorescence quenching is rather small. Using the Smoluchowski diffusion-assisted binary collision model under certain assumptions and approximations, we found that the calculated proton diffusion constant in ice in the temperature range of 240−260 K was 10 times greater than that of water at 295 K.

Introduction

Proton transfer reactions in water, such as acid−base neutralization reactions, excess proton mobility, and proton pumping through membrane protein channels, are extensively studied in the fields of chemistry and biology.[1−4] However, proton reactions in the solid phase, and particularly in ice, are much less studied.[5,6] The physics of ice[7−10] has been studied for a long time, posing many questions that still puzzle us today.[8]

Ice exhibits a high static relative permittivity which is comparable to that of liquid water. Two types of structural defects are mostly responsible for the ice's electrical properties. (1) Ion defects, which are produced when a proton moves from one end of the bond to the other, thus creating a H_3O^+, OH^- ion pair.[11] Conduction is then made possible by means of successive proton jumps (the von Grotthuss mechanism). (2) Bjerrum defects,[12] which are orientational defects caused by the rotation of a water molecule to produce either a doubly occupied bond (D-defect) or a deprotonated bond (L-defect). The mechanism of the excess proton transfer in ice was investigated by Ohmine and co-workers[13] using the QM/MM method. They proposed that in ice the excess proton is localized in an L-defect. Podeszwa and Buch[14] studied the structure and dynamics of orientational defects in ice by molecular dynamics simulations. They found the defect structure to be quite different from the one originally proposed by Bjerrum.[12] For the L-defect, one water molecule is displaced at ∼1 Å from the crystal lattice site. Defect jumps occur via vibrational phase coincidence.

In the early 1960s, it was estimated from the electrical conductivity measurements of Eigen[4,15] that the proton mobility in ice is 10−100 times larger than in water. In numerous further measurements it was found that at about 263 K the proton mobility in ice (0.8×10^{-4} cm^2 V^{-1} s^{-1}) is smaller than in water[16] by about a factor of 2 (when compared to supercooled liquid water[17,18] at the same temperature). The large proton conductivity of ice found in Eigen's experiments was explained as arising from large surface conductivity rather than bulk conductivity.[9] In recent years other techniques were employed to resolve the mystery of proton mobility in ice. The experimental results on the mobility of protons in thin-film ice indicate that proton transport is a thermally activated process that occurs quite slowly in ice at low temperature[5,19−24] or even not at all.[25] In contrast to low proton mobility in low-temperature ice film, recent experimental[26,27] and computational[28] studies on proton translocation along the proton wire of the green fluorescent protein (GFP) indicate that the proton mobility in an ordered proton-conductive array of four molecules is ultrafast and with a concerted mechanism.

Over the last three decades,[29−38] excited-state intermolecular proton transfer (ESPT) to the solvent or to a base in a solution has been widely researched in the liquid phase. In a recent paper,[39] we studied the photoprotolytic cycle of the photoacid 2-naphthol-6,8-disulfonate (2N68DS) in liquid water and in ice in the presence of small concentrations of the strong mineral acid, HCl. When the irradiated sample is in neutral pH, the protonated form, ROH*, exhibits a nonexponential long-time fluorescence tail decay that arises from the diffusion-assisted reversible geminate recombination of the transferred proton with the RO^-*, followed by a second cycle of proton transfer, i.e., $H^+ + RO^-* \rightleftarrows ROH*$. When excess protons are present in liquid and in ice, the long-time fluorescence tail decays nearly exponentially with the lifetime of the deprotonated form, the $RO*^-$. In ice, in the presence of HCl, we found that the exponential fluorescence long-time tail had a surprisingly large amplitude, even in an excess proton concentration as low as a fraction of 1 mM. A kinetic model was used to analyze the experimental time-resolved data. We deduced the proton diffusion constant in ice from the experimental data fit. We found that the proton diffusion in ice I_h at 240−263 K is about 10 times larger than in liquid water at 295 K.

In a subsequent work[39] we studied the fluorescence quenching of flavin mononucleotide (FMN) in liquid water and in ice in the presence of small concentrations of the strong mineral HCl acid. We deduced the proton diffusion constant in ice from the fit of the experimental time-resolved emission data by using the irreversible diffusion-assisted recombination model based on the Debye−Smoluchowski equation. We found that the proton diffusion in ice I_h at 240−263 K is about 10 times larger than in liquid water at 295 K. The large proton diffusion value

* Corresponding author. E-mail: huppert@tulip.tau.ac.il. Tel.: 972-3-6407012. Fax: 972-3-6407491.

10.1021/jp806242a CCC: $40.75
Published on Web 01/15/2009

SCHEME 1

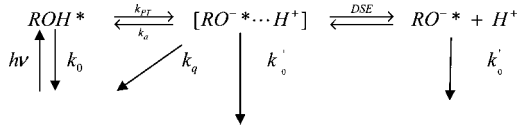

found in our recent studies is in agreement with the findings of Eigen and deMaeyer[40,41] from about 50 years ago.

In the present work we use time-resolved and steady-state methods to study the fluorescence quenching of the RO^- form of the two photoacids 1N4S and 1N3S in ice, in the presence of excess protons that are introduced by adding a strong mineral acid, HCl, at a small concentration range of $0.25 < c < 4$ mM. From the analysis of the experimental results and using certain assumptions, we conclude that the excess proton diffusion constant in ice is roughly 10 times larger than in liquid water at 295 K. The diffusion constants of the proton in ice extracted from the current study are consistent with our previous study,[39] which analyzed the effects of excess protons in ice on the reversible photoprotolytic cycle of photoacids and flavin mononucleotide.

Experimental Section

We used the time-correlated single-photon-counting (TCSPC) technique to measure the time-resolved emission of 1-naphthol derivatives. For sample excitations we used a cavity-dumped Ti:sapphire femtosecond laser, Mira, Coherent, which provides short, 80 fs, pulses. The laser's third harmonics (THG), operating over the spectral range of 260−280 nm, was used to excite both photoacid ice samples. The cavity dumper operated with a relatively low repetition rate of 500 kHz. The TCSPC detection system is based on a Hamamatsu 3809U photomultiplier and Edinburgh Instruments TCC 900 computer module for TCSPC. The overall instrumental response was about 35 ps (fwhm). The excitation pulse energy was reduced to about 10 pJ by neutral-density filters.

1-Naphthol-4-sulfonate (1N4S) and 1-naphthol-3-sulfonate (1N3S) (+95%) were purchased from TCI. HCl (1N) was purchased from Aldrich. For transient measurements the sample concentrations were between 2×10^{-4} and 2×10^{-5} M. Deionized water had a resistance of >10 MΩ. Methanol of analytical grade was purchased from Fluka. All chemicals were used without further purification.

The temperature of the irradiated sample was controlled by placing the sample in a liquid N_2 cryostat with a thermal stability of approximately ±1.5 K.

Ice samples were prepared by first placing the cryogenic sample cell for about 20 min at a supercooled liquid temperature of about 260 K. The second step involved a relatively rapid cooling (5 min) to a temperature of about 250 K. Subsequently, the sample froze within a few minutes. To ensure ice equilibration prior to the time-resolved measurements, the sample temperature was kept for another 10 min at about 250 K.

Reversible and Irreversible Photoprotolytic Cycle of Photoacids. 1-Naphthol and its derivatives are known to exhibit large fluorescence quenching of the deprotonated form, RO^-, in acidic aqueous solutions. Scheme 1[31] describes the photoprotolytic cycle that includes also proton quenching. Within a few hundred femtoseconds, excitation of a solution at pH values lower than the ground-state pK_a of photoacids in general and of 1-naphthol derivatives in particular generates a vibrationally relaxed, electronically excited ROH molecule (denoted by R*OH). Proton dissociation, with an intrinsic rate constant k_{PT}, leads to formation of the contact ion pair $R^*O^-\cdots H^+$, whereas adiabatic recombination with rate constant k_a may reform the excited acid. In general, back protonation may also proceed by a nonadiabatic pathway, involving proton quenching with a rate constant k_q. Separation of an anion pair from the contact radius, a, to infinity is described by the transient numerical solution of the Debye−Smoluchowski equation (DSE).[34] Additionally, one should consider the fluorescence lifetimes of all excited species, $1/k_0 = \tau_0$ for the acid, and $1/k'_0 = \tau'_0$ for the base. Usually, k_0 and k'_0 are much slower than all chemical and diffusion processes.

The Smoluchowski Model. The Smoluchowski model is used to describe the diffusion-assisted irreversible reaction A + B → AB, where the concentration of B is in a great excess over A. In this study, it is used to fit the time-resolved emission decay of the base form, RO^-, of the 1-naphthol derivatives in the presence of an excess proton in the ice sample.

We assumed that the excess proton transport toward the RO^- is the rate-limiting step. The mathematical and computational details of the Smoluchowski model are given elsewhere.[42] According to the Smoluchowski model, the survival probability of a single (static) donor, an excited RO^- molecule (the A particle), due to its irreversible reaction with a $c = [H^+]$ concentration of protons (B is the excess proton in liquid and ice) is given by[43−45]

$$S(t) = \exp(-c \int_0^t k(t')\, dt') \tag{1}$$

where $k(t)$ is the time-dependent rate coefficient for the donor−acceptor pair

$$k(t) = k_a p(a,t) \tag{2}$$

whose intrinsic proton-recombination rate constant is k_a. The pair (RO^-/H^+) density distribution, $p(r,t)$, is governed by a three-dimensional Smoluchowski equation (diffusion in a potential $U(r)$).[46]

When $U(r) = 0$, the above equations are analytically solvable for $k(t)$.[44] Szabo[45] found an approximate expression for the time-dependent rate constant for the instances when $U(r) \neq 0$.

When a potential is introduced, it behaves correctly at both $t = 0$ and $t = \infty$; i.e.

$$k(0) = k_{PT} e^{-\beta U(a)}, \quad k(\infty) = [k(0)^{-1} + k_D^{-1}]^{-1} \tag{3}$$

where

$$k_D = 4\pi D a_e \tag{4}$$

is the diffusion-controlled rate constant, and a_e is an effective radius that depends on the Coulomb pair attraction potential. $U(a)$ and a_e depend on the dielectric constant[34] with

$$a_e = R_D/(1 - \exp(-R_D/a)) \tag{5}$$

and

$$R_D = \frac{ze^2}{\varepsilon_s k_B T} \tag{6}$$

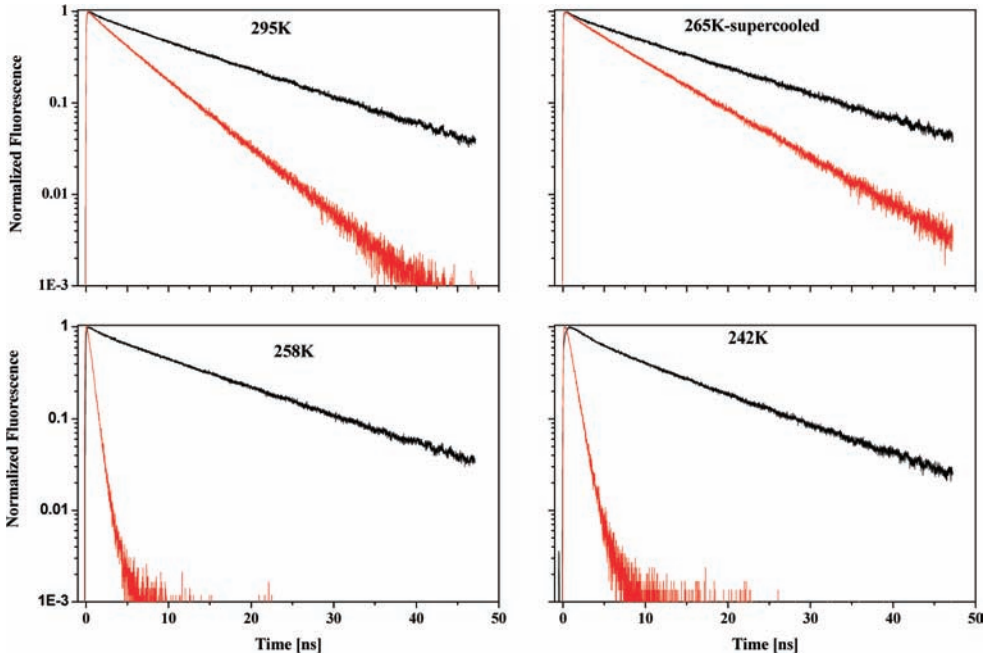

Figure 1. Time-resolved emission of RO^- of 1N4S in a 0.1% methanol-doped aqueous sample at several temperatures. Each frame contains two samples: a neutral pH sample and a sample that contains 4 mM HCl.

where a is the actual encounter radius of the specific reaction. $a = 7$ Å is a commonly used value for a proton reaction in aqueous solutions.[3] R_D is the Debye radius, z is the charge of the molecule in electronic units and e is the charge of the electron. The value of a_e for 1N4S in its RO^{*-} form in water with a dielelectric constant of $\varepsilon_s = 78$ is 16 Å. In ice, where we assume $\varepsilon_s = 100$, it is 12.5 Å.

The nonexponentiality in $S(t)$ is a result of a time-dependent rate constant, $k(t)$, as depicted by the ratio $k(0)/k(\infty) = 1 + k(0)/k_D$.

Results

Figure 1 shows the time-resolved emission of the RO^- of 1N4S in methanol-doped ice of two samples: that of a neutral pH and that of a sample that contains 4 mM HCl. The methanol doping was 0.1% mole ratio. The figure shows the time-resolved emission of liquid samples as well as solid samples at several temperatures. The signal's decay rates of the neutral and the acidic samples differ strongly in ice, but in the liquid state the decay rate of the 4 mM HCl sample is much smaller. In ice, the acidic sample's time-resolved signal decay rate is large and nonexponential. In an irreversible proton recombination process

$$A^- + H^+ \xrightarrow{k_{irr}(t)} AH$$

where $[H^+]$ is in large excess (based on the Debye−Smoluchowski equation), the excess proton reaction rate constant assumes the value of $k(0) = k_a \exp[-\beta U(a)]$ at short times, while at long times it becomes $k(\infty) = [k(0)^{-1} + k_D^{-1}]^{-1}$ (see eq 3), where $k_D = 4\pi N' R_D D_{H^+}$ is a bimolecular, diffusion-controlled rate constant in units of M^{-1} s^{-1}. When $k(0) > k_D$ then $k(\infty) \approx k_D$. In the latter case the constant flux of protons toward the target controls the reaction rate. From the decay rate of the fluorescence signal of the RO^- form of 1N4S in the acidic sample one can estimate the proton diffusion constant.

Figure 2a shows the time-resolved emission of the protonated form, ROH, of 1N4S in 0.1% (mole ratio) methanol-doped ice samples that contain 4 mM HCl and of samples with a neutral pH. The figure shows that in the liquid state the effect of 4 mM of acid on the time-resolved emission of the ROH is rather small. The fluorescence decay signals of the acid-free sample and of that with an acid concentration of 4 mM overlap from early times up to about 1/100 of the peak intensity. In the ice, the decay of the sample that contains 4 mM of HCl overlaps the neutral pH signal only at early times. Later on, after about 300 ps, its decay is slower and clearly deviates from that of the neutral pH solution. The explanation for the small, but distinct, acid effect is as follows: in water, the proton transfer is fast whereas the proton diffusion is relatively small, and thus, the reversible (adiabatic) reprotonation reaction

$$RO^{-*} + H^+ \xrightarrow{k_a} ROH^*$$

by excess protons is only effective at long-times. Furthermore, it competes with the irreversible (nonadiabatic) reaction

$$RO^{-*} + H^+ \xrightarrow{k_q} ROH$$

In ice at 250 K, the excited-state proton transfer rate is slower by a factor of 5 than in water at 295 K. The reversible reprotonation rate, however, is large since the proton diffusion constant in ice is large. Thus, reprotonation of the hydroxyl group by excess protons takes place, and 300 ps after excitation the signal deviates from the neutral pH. This is also the time scale of the fluorescence quenching decay rate of the RO^{-*} signal, which is a result of the protons' reaction with the carbons at the distal ring. Figure 2b shows our attempt to fit the neutral pH experimental data by solving the DSE with reversible and irreversible geminate proton recombination, using the SSDP program.[47] The fitting parameters are given in Table 1. As seen in the figure, we get a good fit for the experimental data in both liquid and the solid phases.

In 1-naphthol derivatives the irreversible fluorescence quenching reaction (Scheme 1) is much more efficient than for 2-naphthol derivatives.[31]

As seen in the Figure 2a, at 4 mM of HCl in ice the time-resolved fluorescence signal of ROH is almost the same as the neutral pH. The fluorescence long-time tail arises from the

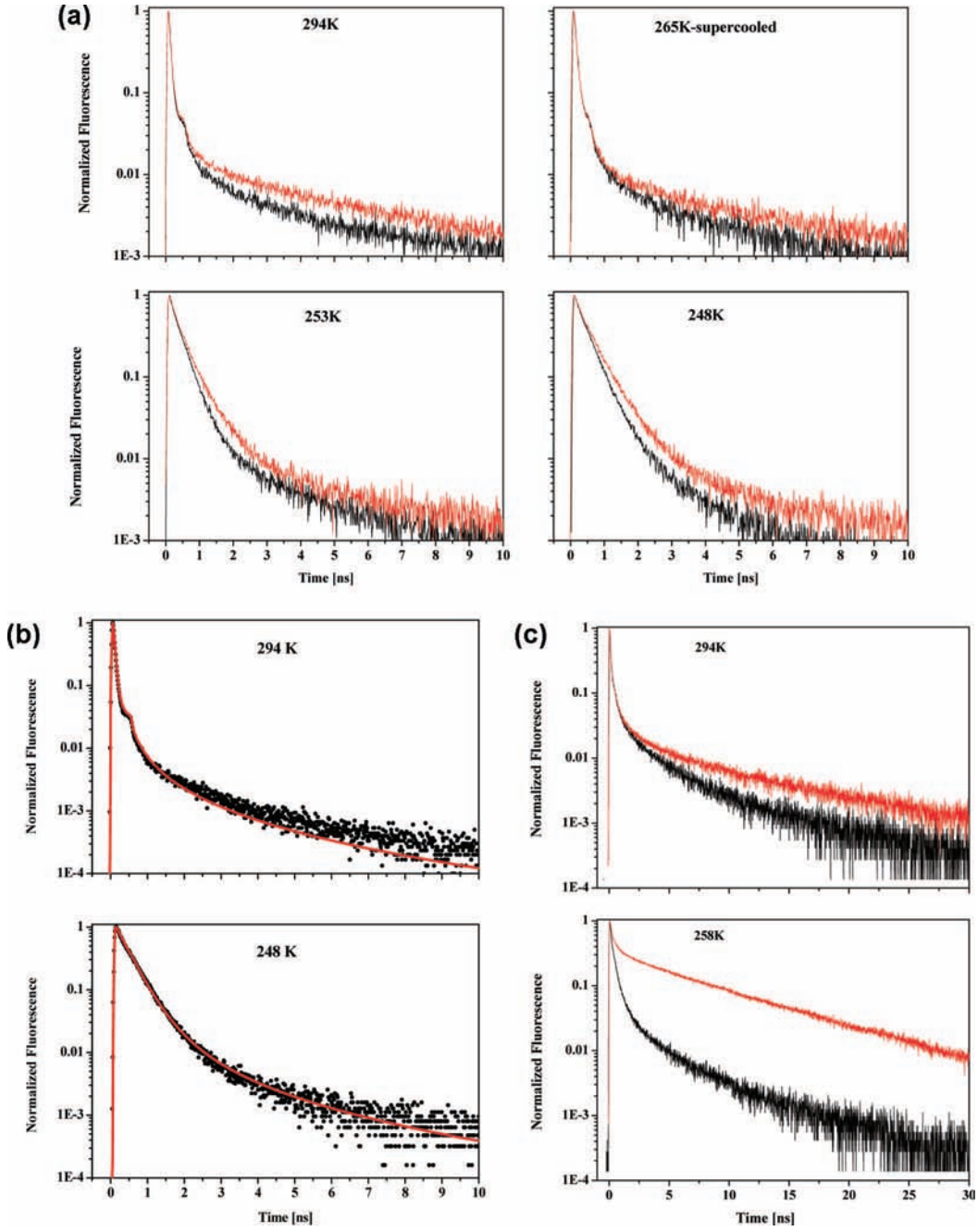

Figure 2. Time-resolved emission of the ROH form of photoacids in a 0.1% methanol-doped aqueous sample at several temperatures: (a) 1N4S; (b) fit to the ROH data in neutral pH sample of 1N4S using the photoprotolytic model (see text); (c) 2N68DS.

reversible (adiabatic) geminate recombination reaction that competes inefficiently with the irreversible proton reaction. The reversible reaction is much more efficient in 2-naphthol derivatives, for which the irreversible reaction is inefficient. Figure 2c shows the time-resolved emission of the ROH* form of 2-naphthol-6,8-disulfonate with and without 1 mM of HCl in water and in ice. In 2-naphthol-6,8-disulfonate, where the proton quenching process is ineffective, the amplitude of the long-time fluorescence tail in ice is very large. In our previous study,[39] we deduced the proton diffusion constant in ice from the large amplitude of the long-time fluorescence tail of an acidic sample of the ROH* form of 2N68DS (see Figure 2c) arising from the reversible proton recombination process.

Figure 3 shows the time-resolved emission of the deprotonated form, RO^-, of 1N4S in the presence of 4 mM HCl acid

TABLE 1: Fitting Parameters of the Photoprotolytic Cycle of 1N4S in Acid-Free Samples Using the Geminate Recombination Model[a]

phase	T (K)	k_{PT} (10^9 s^{-1})[b]	k_r (10^9 Å s^{-1})[b,c]	k_g[d] (10^9 Å s^{-1})	D (10^{-5} cm^2 s^{-1})	R_D (Å)
liquid	296	26	12	0.04	7.0	14.6
liquid	278	15	6.5	0.50	5.0	14.6
supercooled	265	15.5	5.0	0.04	3.5	14.6
solid	268	12.5	4.0	0.50	5.0	14
solid	263	8.5	2.8	0.50	5.0	14
solid	258	6.5	2.8	0.50	5.0	14
solid	253	4.9	3.5	3.5	4.0	14
solid	248	3.5	3.5	3.5	4.0	14

[a] The excited-state lifetime of 1N4S, τ = 14.7 ns. [b] Proton transfer rate constant. [c] Reversible recombination rate constant. [d] Irreversible recombination rate constant.

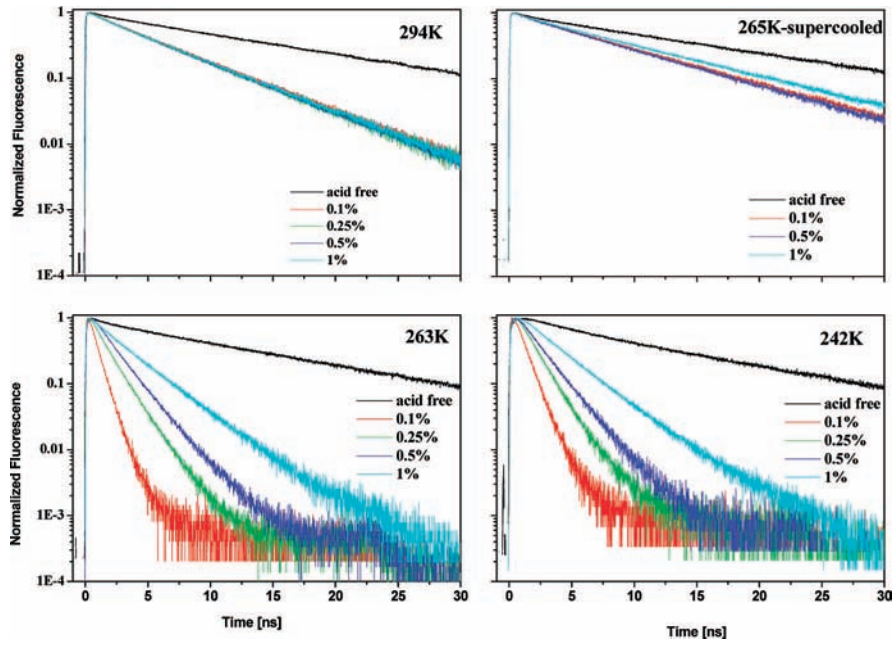

Figure 3. Time-resolved emission of RO^- of 1N4S in 4 mM HCl at various methanol doping concentrations, measured at different temperatures. The methanol concentrations are 0.1%, 0.25%, 0.5%, and 1% mole ratio.

in methanol-doped ice samples that differ in their methanol concentrations. As seen in the figure, the lower the methanol concentration, the larger the quenching rate. The fluorescence quenching decay arises from the reaction of the excess proton in ice with excited-state RO^-* to form the ground state, ROH. The overall rate constant depends on both the proton diffusion-controlled rate and the intrinsic proton recombination rate. There is a large dependence of the quenching rate of the RO^-* on the methanol concentration. When the methanol concentration is about 1% mole ratio, the proton quenching rate is smaller by a factor of 5 than its value at 0.1% mole ratio of methanol. A probable explanation to this effect would be that the methanol molecules trap the mobile proton in the bulk ice. An alternative explanation to the methanol effect is as follows: methanol tends to preferentially solvate the naphthol's aromatic rings. It is well-known that in pure methanol both the proton transfer to the solvent and the reverse proton recombination reaction rates of photoacids decrease by several orders of magnitude. The methanol in the methanol-rich aqueous solutions used in this study, may form a thin solvation layer surrounding the naphthol, and consequently, the intrinsic proton recombination rate decreases in highly doped ice.

Figure 4 shows a comparison between the time-resolved emission of RO^-* of 1N4S with the same level of methanol doping (0.1% mole ratio) at three particular points: (a) ice at 258 K containing 4 mM acid, (b) a sample of the same composition in the supercooled liquid at 265 K, and (c) ice close to the melting point at 268 K. As seen in the figure, the supercooled liquid sample fluorescence decay rate is the smallest and similar to the signal decay of a liquid sample at temperatures above freezing point, whereas in the solid sample at 258 K, the decay rate is more than 10 times larger. The time-resolved emission of RO^-* of 1N4S in the presence of acid in methanol-doped ice samples at 268 K shows a much smaller quenching rate than ice at temperatures below 258 K. The proton diffusion constant at 268 K is about one-third of its value at lower temperatures. A similar finding was also observed in our previous studies[39] on the excess proton effect on the reversible photoprotolytic cycle of 2N68DS and on the proton quenching of flavin mononucleotide.

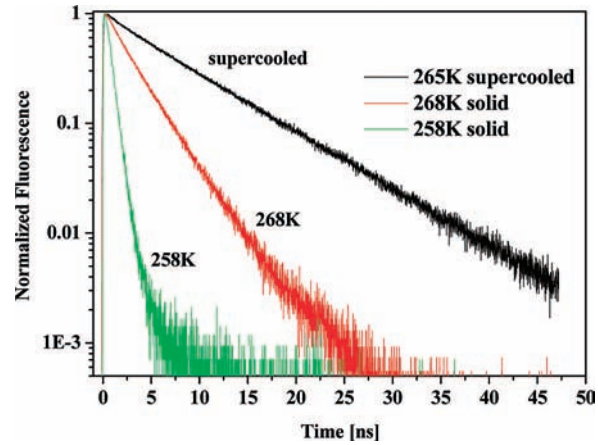

Figure 4. Time-resolved emission of 1N4S in 4 mM HCl in 0.1% methanol-doped samples, in the solid phase and in a supercooled liquid sample at about the same temperature and for comparison also shown an ice sample at 258 K.

Figure 5 shows the time-dependent fluorescence of the RO^-* of 1N4S in methanol-doped ice (0.1% by mole ratio) at several HCl concentrations in the range of 0.25−4 mM. As seen in the figure, at all acid concentrations the signal decay rate is much larger than in ice in the liquid phase. The decay rate depends on the acid concentration in both liquid and ice. The larger the acid concentration, the larger the quenching rate.

Figure 6 shows the fit of the experimental results of the RO^-* of 1N4S time-resolved fluorescence to the diffusion-assisted kinetic model of $A + B \rightarrow AB$, using eqs 1−3. The model fits the short- and the long-time signal reasonably well at methanol doping in the range of 0.1% mole ratio to larger values. In general, the lower the temperature and the methanol-doping level, the larger the nonexponential character of the experimental results. To get a better fit for the short-time signals, we introduced a generation function to mimic the generation of the RO^-* from the excited photoacid ROH* by transferring the hydroxyl proton to the solvent. The rate of the proton transfer (PT) from photoacid to water or ice strongly depends on the temperature. For samples at room temperature the PT rate

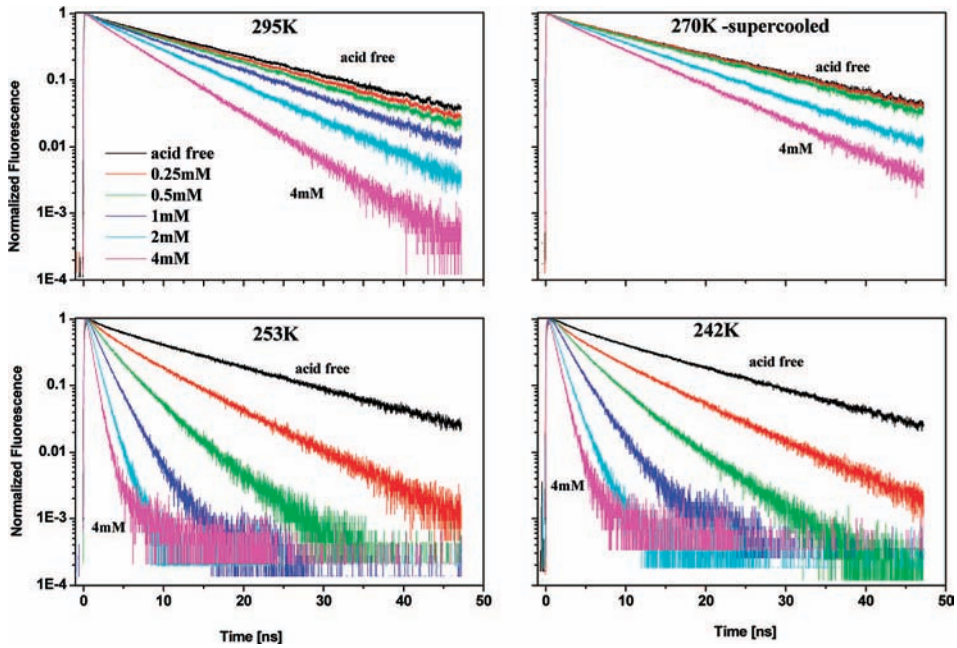

Figure 5. Time-resolved emission of the RO^-* of 1N4S in 0.1% mole ratio of methanol−water samples at several HCl concentrations in the range of $0.25 < c < 4$ mM. Each frame shows the results of a certain temperature.

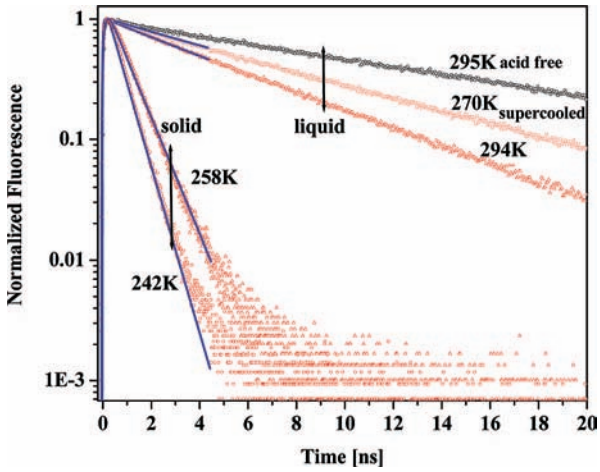

Figure 6. Experimental data and computer fits using the Debye−Smoluchowski irreversible model of the time-resolved emission of the RO^- of 1N4S in 4 mM HCl, measured at different temperatures.

constant is 3×10^{10} s^{-1}, whereas at 247 K it is about 5×10^9 s^{-1}. The model's calculated fit is almost exponential at times larger than 50 ps. The time-dependent rate constant $k(t)$ of the Smoluchowski model varies from the initial value of $k(0)$ at time zero to $k(\infty)$ at a longer time. Since in ice k_D is large because $D = 10^{-3}$ cm^2/s, the switching between $k(0)$ and $k(\infty)$ occurs in a very short time span.[42] The survival probability $S(t)$ also depends on the proton concentration c, which in our experiments is low. Under such conditions, $S(t)$ basically follows $k(\infty)$ after about 50 ps and the well-known nonexponential behavior of the Smoluchowski theory is hardly observed at longer times.

The observed nonexponential RO^-* fluorescence decay of 1N4S is likely to arise from a large dispersion in the transport properties of the protons in ice, rather than from the nonexponential decay predicted by solving the DSE. Ordered proton wires of various lengths promote large diffusion constants.[48] Ice is a disordered system with a large concentration of defects. Methanol doping introduces proton traps in the bulk ice. Trapped protons may be released over a long time span and thus protons may hit the target molecules (RO^-* of 1N4S) at different times. The fitting parameters of the diffusion-assisted irreversible proton recombination model of several samples are given in Tables 2−5.

The values of the proton diffusion constant in ice obtained for neutral pH samples and the one obtained for acidic samples vary by a factor of 10. In the neutral pH, ice sample we used the reversible geminate recombination model for the fit of the experimental time-resolved emission mainly that of the ROH band, whereas for the acidic ice samples we used the irreversible Smoluchowski model to fit the RO^- band. In the neutral pH

TABLE 2: Fitting Parameters of the Proton Quenching of RO^- in 4 mM HCl, 0.1% Mole Fraction of Methanol-Doped Water and Ice[a]

phase	T (K)	k_0 (10^{11} s^{-1})	D (10^{-4} cm^2 s^{-1})	R_D (Å)
liquid	294	0.6	0.75	14
supercooled	265	0.6	0.3	14
solid	268	5.0	6.0	14
solid	258	5.0	14	14
solid	253	5.0	20	14
solid	247	5.0	16	14
solid	242	5.0	11	14
solid	237	5.0	8	14

[a] The excited-state lifetime of 1N4S, $\tau = 14.7$ ns.

TABLE 3: Fitting Parameters of the Proton Quenching of RO^- in 4 mM HCl, 0.25% Mole Fraction of Methanol Doped Water and Ice[a]

phase	T (K)	k_0 (10^{11} s^{-1})	D (10^{-4} cm^2 s^{-1})	R_D (Å)
liquid	294	0.6	0.7	14
liquid	278	0.6	0.3	14
supercooled	265	0.6	0.4	14
solid	268	1.0	2	14
solid	263	2.7	5	14
solid	258	2.7	10	14
solid	253	2.7	10	14
solid	247	2.7	8	14
solid	242	2.7	5	14

[a] The excited-state lifetime of 1N4S, $\tau = 14.7$ ns.

TABLE 4: Fitting Parameters of the Proton Quenching of RO^- in 4 mM HCl, 0.5% Mole Fraction of Methanol-Doped Water and Ice[a]

phase	T (K)	k_0 (10^{11} s^{-1})	D (10^{-4} cm^2 s^{-1})	R_D (Å)
liquid	294	0.6	0.75	14
liquid	278	0.6	0.5	14
supercooled	265	0.6	0.3	14
solid	268	1.0	0.9	14
solid	263	1.8	3.25	14
solid	258	1.8	4.25	14
solid	253	1.8	4.25	14
solid	247	1.8	4.25	14
solid	242	1.8	4.25	14

[a] The excited-state lifetime of 1N4S, $\tau = 14.7$ ns.

TABLE 5: Fitting Parameters of the Proton Quenching of RO^- in 4 mM HCl, 1.0% Mole Fraction of Methanol-Doped Water and Ice[a]

phase	T (K)	k_0 (10^{11} s^{-1})	D (10^{-4} cm^2 s^{-1})	R_D (Å)
liquid	294	0.6	0.67	14
supercooled	265	0.8	0.35	14
solid	268	1.3	0.95	14
solid	263	1.3	1.7	14
solid	258	1.3	2.3	14
solid	253	1.3	2.3	14
solid	247	1.3	2.2	14
solid	242	1.3	1.8	14
solid	232	1.3	1.2	14

[a] The excited-state lifetime of 1N4S, $\tau = 14.7$ ns.

samples the proton geminate recombination rate mainly covers RO^-/H^+ distances that are rather short, i.e., up to about 30 Å. In the acid experiments the average RO^-/H^+ distance is ~100 Å. We expect that the structure of water molecules next to the photoacid is far from a perfect ice I_h crystal structure. The methanol concentration in the close vicinity of the acid may be larger than the homogeneous concentration. In such an undefined ice structure, one expects that the proton diffusion is much smaller than in a well-defined ice I_h structure. We therefore explain the large difference in proton diffusion constants obtained from the two samples by the large difference in the H^+/RO^- distances of the traveling proton. In the acid samples, a proton may travel 500 Å within 10 ns, whereas in the case of geminate recombination of a proton that is first released from the ROH*, it covers much shorter distances. The geminate proton senses the disordered region of ice next to a large structural defect for which the proton diffusion constant is rather small.

Figure 7 shows the time-resolved emission of the ROH form of 1N3S measured at 360 nm for several temperatures. In each frame there are two decay curves; the signal of neutral sample and a sample that contains 4 mM HCl. As in the case of 1N4S, the acid effect is rather small on the time-resolved emission of the ROH. The proton transfer rate of 1N3S to the solvent at a particular temperature is smaller than that of 1N4S. The relatively small proton transfer rate of 1N3S at low temperatures as well as the relatively shorter lifetime of its RO^- emission band (7 ns) prevents the accurate measurements of the proton diffusion constant in ice at low temperatures.

Figure 8 shows the time-resolved emission of the RO^- form of 1N3S measured at 460 nm for several temperatures. Each frame shows the signal of a neutral pH solution and of a sample that contains 4 mM HCl. The decay rate of the RO^- signal of the ice samples that contain 4 mM acid is large whereas in the liquid state the decay rate of the 4 mM is much slower than in the ice phase but shorter than in the neutral pH solution. In general, the results of 1N3S are similar to those of 1N4S for which we conducted a much more detailed analysis. The values of the proton diffusion constant as a function of the temperature in 0.1% mole ratio of methanol-doped ice are given in Table 6. The values of the diffusion constant are about 50% smaller than the one found for 1N4S. We used for 1N4S and 1N3S the same value of the intrinsic rate constant k_0. 1N3S is a weaker photoacid than 1N4S. The value of k_0 is arbitrarily chosen to be larger than k_D. It is plausible that in 1N3S $k_0 < k_D$, and in such a case, the rate-limiting step is k_0 and not the proton diffusion process. Therefore, the calculated diffusion constant is relatively smaller than that derived from the 1N4S experiments, where $k_0 > k_D$.

Discussion

Proton mobility in cold thin films indicates that it is a thermally activated process with a large activation energy. Proton conductivity measurements by Takei and Maeno[55,56] on large single ice crystals doped with HCl indeed show that below 220 K the ac conductivity, σ_∞, exhibits an activation energy of ~0.31 eV.[10,56] The thin film experimental results suggest that protons are mobile through the ice film in both amorphous ($T < 140$ K) and crystalline phases ($T \geq 140$ K) that form during the course of the temperature ramp. In addition, it has been observed[49] that Cl^- ions produced from HCl dissociation do not migrate to the surface of film at $T \leq 140$ K, while protons build up a substantial population at the surface. This shows that the upward migration of proton is not caused by the presence of counteranions. Kang et al.[24] suggest that the anomalous experimental reports on the mobility of protons in ice films[5,19−21,25,50] can be explained by the affinity of protons for the ice surface and the facile proton transport near the surface at $T \geq 130$ K. The result verifies that protons are mobile in an ice film and can migrate from the film interior to the surface at favorable temperatures. This conclusion is unaffected by the changes in ice film morphology and thickness (2−8 BL) and by the presence of counteranions.

More than twenty years ago we measured the reaction of a proton with the ground-state conjugate base of pyranine in pure ice,[51] $RO_{(g)}^- + H^+ \rightarrow ROH_{(g)}$. We found that the recombination rate is on a microsecond time scale. The proton diffusion constant was estimated to be about half of that of liquid water as expected from the conductivity measurements of refs 16 and 17. This work is our third study devoted to measuring proton diffusion in methanol-doped ice. All the studies are based on time-resolved emission measurements, where a probe molecule is photoexcited and its reactivity is drastically changed. In our first work,[39] the probe molecule was a common reversible photoacid 2-naphthol-6,8-disulfonate. The first step in the photoprotolytic cycle is a proton transfer from the ROH* to the solvent. The proton diffuses in liquid water or in ice and may recombine geminately to reform the excited photoacid ROH*. An excess proton in solution (introduced by adding of a strong acid to the sample) can also react with the conjugate base, the RO^-*, to reform the ROH*. In the absence of excess protons in liquid water and in ice, the reversible diffusion-assisted photoprotolytic cycle is characterized by a nonexponential long-time fluorescence tail of the ROH*.[52,53] In samples that contain excess protons due to the addition of a strong acid, like HCl, the long-time fluorescence tail becomes exponential with the lifetime of the deprotonated form, the RO^-*. The amplitude of the exponential tail, which depends on the proton diffusion constant, increases linearly with the strong acid

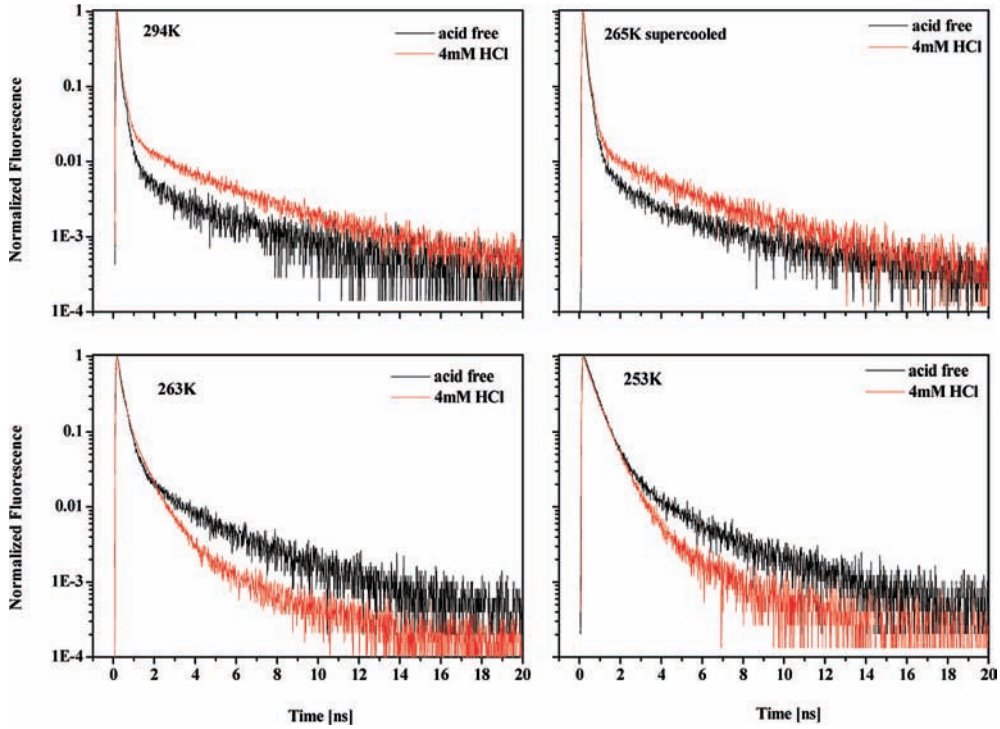

Figure 7. Time-resolved emission of the ROH of 1N3S in 0.1% mole ratio of methanol−water samples in neutral pH and 4 mM HCl.

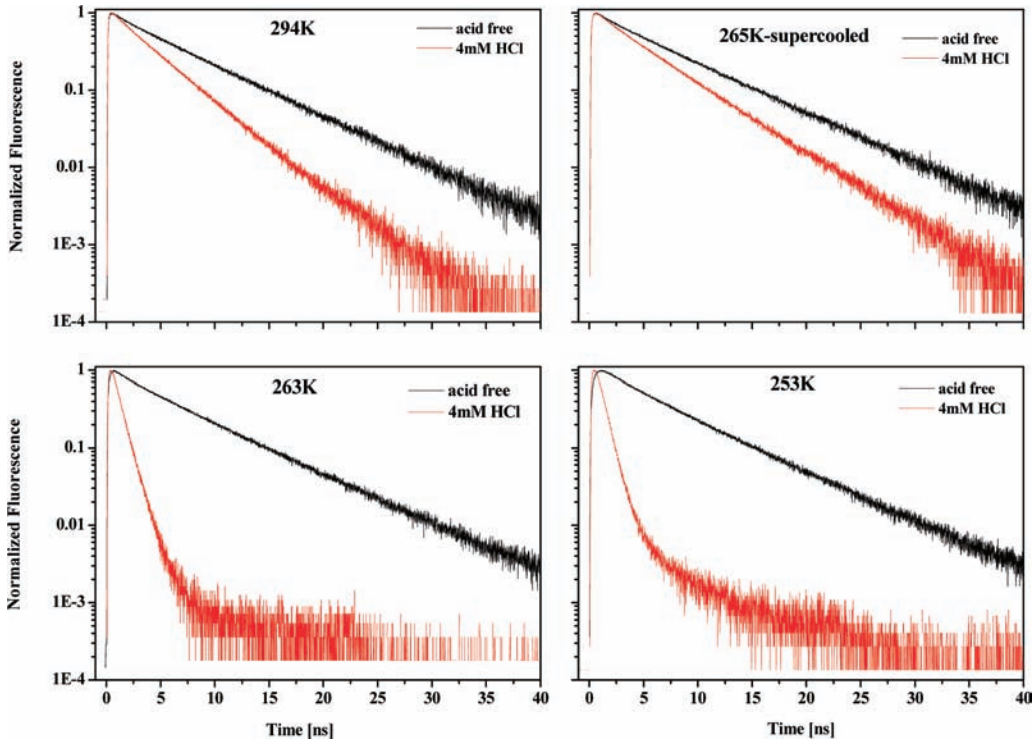

Figure 8. Time-resolved emission of the RO^- of 1N3S in 0.1% mole ratio of methanol−water samples in neutral pH and 4 mM HCl.

concentration. In ice, the amplitude of the ROH long-time exponential fluorescence tail is 10 times larger than in water; consequently, we deduced that the proton diffusion constant in ice is 10 times larger than in water.

In our second work,[39] we measured the fluorescence quenching of flavin mononucleotide (FMN) in a proton-rich aqueous solution and in ice. Quenching probably took place when the proton reacted with one of the four heterocyclic nitrogens of the excited flavin molecule. In ice, the lifetime became shorter by a factor of 10 as compared to the liquid state. Our conclusion from these FMN experiments was in agreement with our first study that the proton diffusion constant in ice is 10 times greater than in the liquid state.

In the current study, we used as probe molecules two 1-naphthol derivatives: 1N4S and 1N3S. Excited 1-naphthol and its derivatives are strong photoacids, $pK^*_a \approx 0$. The first step is an excited-state proton transfer to the solvent. In liquid water at room temperature, the proton transfer rate constant roughly equals 3×10^{10} s^{-1}. The second step of the photoprotolytic cycle involves a diffusion of the proton in the medium and the

TABLE 6: Fitting Parameters of the Proton Quenching of RO^- of 1N3S in 4 mM HCl, 0.1% Mole Fraction of Methanol-Doped Water and Ice[a]

phase	T (K)	k_0 (10^{11} s^{-1})	D (10^{-4} cm^2 s^{-1})	R_D (Å)
liquid	294	0.5	0.90	14
solid	268	3.0	2.50	14
solid	263	5.0	8.50	14
solid	258	5.0	11.00	14
solid	252	5.0	9.00	14
solid	248	5.0	9.00	14
solid	242	3.0	6.50	14

[a] The excited-state lifetime of 1N3S, $\tau = 7.0$ ns.

finite probability to geminately recombinate with the RO^-*. In the case of 1-naphthols, the proton recombination process is subdivided into two processes. The first one is a reversible (adiabatic) process to reform the excited-state ROH*, which may subsequently undergo a second photoprotolytic cycle. The second one is an irreversible (nonadiabatic) reaction of the proton with the RO^-* to create a ground-state ROH. This reaction leads to the fluorescence quenching of the RO^-*, and the end result is an increase of the decay rate of the RO^-* fluorescence at short times. As in the two previous experiments, the time-resolved emission of the 1-naphthol derivatives in ice is strongly modified as compared to that in liquid water.

The main findings of the present study are as follows:

1. An excess of protons in ice, introduced by adding a strong mineral acid, reacts with the excited anionic RO^-* form of 1-naphthol sulfonate derivatives. As a result, the fluorescence lifetime of the RO^-* is reduced.

2. There is a rather weak temperature dependence of the fluorescence quenching rate in ice in the range of 230−263 K.

3. The fluorescence quenching rate of the RO^-* in methanol-doped ice inversely depends on the methanol concentration. The smaller the methanol concentration the larger the quenching rate.

The discussion on the results of this study includes two different explanations to the large excess proton fluorescence quenching effect in ice that was observed. The first explanation is given below. It is based on a homogeneous solution chemistry that takes place in the bulk of a microcrystal in polycrystalline ice. The second explanation is based on the assumption that ice is a bad solvent, and that the photoacid is positioned at the grain boundaries or at the surface layer of the microcrystal.

Assumptions and Approximations of the First Model. The main assumptions are as follows:

1. Both the photoacid molecules and the protons are homogeneously distributed in the bulk of the polycrystalline samples. HCl is a strong acid. Therefore, the degree of acid dissociation is almost 1, and the proton concentration is close to the HCl concentration introduced into the aqueous solution.[54]

2. The methanol molecules serve as a cosolvent that prevents the exclusion of the 1-naphthol derivatives from the bulk ice. The methanol hydrophobic CH_3 group points toward the aromatic rings of the 1-naphthol derivatives, whereas the sulfonate and the hydroxyl group form hydrogen bonds with the hydrogen bond network structure in the ice.

3. The high value of the dielectric constant of pure ice is maintained even when the ice is doped with a range of acid concentrations ($0.25 \le c \le 4$ mM) of HCl. At the freezing point the large dielectric constant of roughly $\varepsilon = 100$ further increases as the temperature decreases.

The long-time asymptotic expression for the irreversible rate constant takes into account both the diffusion-controlled rate constant and the intrinsic rate constant $k(\infty) = [k(0)^{-1} + k_D^{-1}]^{-1}$ (see eq 3). From the time-resolved measurements of 1N4S in both liquid and in ice, the intrinsic quenching rate constant $k(0)$ (eq 3) at 260 K is about 6×10^{11} M^{-1} s^{-1}. For a diffusion constant of 10^{-3} cm^2/s and a large dielectric constant ($\varepsilon = 100$), the second order diffusion-controlled rate is 5×10^{11} M^{-1} s^{-1}. Thus, the overall rate constant, $k(\infty)$, is about half of k_D.

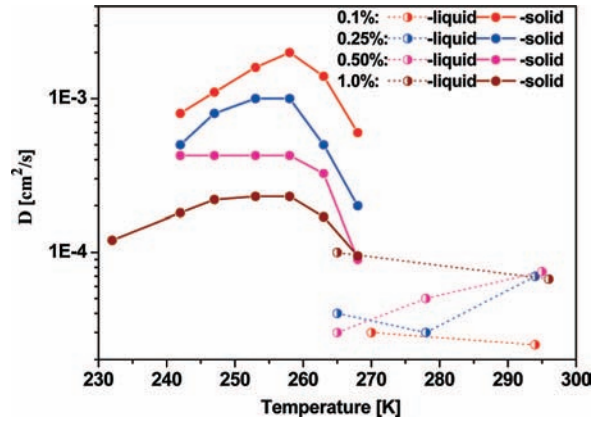

Figure 9. Proton diffusion constant in both water and ice as a function of temperature at several methanol doping levels at different temperatures.

Parameters Affecting the Proton Diffusion Constant. Figure 9 shows a plot of the proton diffusion constant of several samples with different doping levels of methanol as a function of temperature in liquid and in ice. At a very low methanol concentration of 0.1% (mole ratio), the proton diffusion constant reaches a value of $\sim 1.5 \times 10^{-3}$ cm^2/s at about 258 K. As the methanol concentration increases, the diffusion constant decreases. In 1% mole ratio of methanol the diffusion constant drops by a factor of 6 to a value of 2.5×10^{-4} cm^2/s. At 295 K the value of the proton diffusion constant in pure water is much smaller, about 0.9×10^{-4} cm^2/s. From the Smoluchowski diffusion-assisted irreversible recombination model fitting, we were able to deduce a diffusion constant of about 0.35×10^{-4} cm^2/s for the supercooled liquid at 265 K. The value of proton diffusion in an ice sample, doped with a 0.1% mole ratio of methanol, is roughly 40 times larger than the value of the supercooled liquid sample and about 15 times larger than its value at 298 K.

We measured the 1N4S fluorescence intensity in 0.1% mole ratio methanol-doped samples in the presence of HCl in a relatively large concentration range of 0.25−4 mM. We found that in the temperature range of 247−298 K, the diffusion constant obtained from the fit of the experimental data by the Smoluchowski diffusion-assisted irreversible recombination model is independent of the acid concentration, in particular methanol-doped ice samples.

The analysis of the signals of ice at several temperatures shows that the diffusion constant is the largest at 250−260 K. In large methanol concentrations, it decreases at both higher and lower temperatures. At about 268 K, the proton diffusion constant abruptly drops to nearly one-third of its maximum value at 260 K. At very low temperatures ($T < 220$ K), the small proton transfer rate of the protonated form, ROH, in neutral pH samples at low methanol concentrations and low temperatures prevents the accurate determination of the proton diffusion. We estimate that the proton diffusion constant at 230 K is about half of its maximum value.

The small temperature dependence of the diffusion constant is also apparent in the conductivity of the ion defect $\sigma_\pm/e_\pm$ of the HCl-doped sample measured by Takei and Maeno.[55,56] Their

results show that the conductivity is almost constant in the high temperature range of $T > 230$ K, whereas at lower temperatures of $T < 220$ K it obeys an Arrhenius activation behavior, with a large activation energy of 0.3 eV.

In the previous studies, as in this one, we found that the proton diffusion constant of methanol-doped ice strongly depends on the methanol concentration. The value of the proton diffusion constant in ice is much larger than the supercooled liquid values. In the liquid state the diffusion constant weakly depends on the level of the methanol doping. However, in ice this dependence has an inverse relationship: as the methanol concentration increases, the diffusion constant decreases. It increases by a factor of about 6 when the methanol concentration decreases from 1% to 0.1% mole ratio. We explained this effect by the ability of methanol to capture the proton quickly and to release it at a much slower rate. Thus, the methanol traps the proton within the experimental time window. The overall effect is a reduction in the effective diffusion constant within the methanol-doped ice crystal. Methanol doping is necessary to incorporate the photoacid in the crystal bulk and to prevent the exclusion of the photoacid from the bulk and its aggregation at the grain boundaries.

Comparison of the Experimental Results on Proton Diffusion in Ice. Three different experiments based on photochemical reactions and designed to deduce the proton diffusion in ice show conflicting results. There are three kinds of experiments from which we extracted the proton diffusion constant. The first experiment, whose results were published more than 20 years ago,[51] was based on the reaction rate of excess protons in ice with a deprotonated ground-state form of pyranine, RO^-, generated by a photoprotolytic cycle, $ROH^* \rightleftarrows RO^{-}{}^* + H^+$. The short-time after excitation is not observed in this experiment since we followed the ground-state RO^-, and the detection system had a time resolution of about 20 ns.

The observed reaction rate was in the microsecond time scale. The analysis of the second-order reaction rate provided a value of 4×10^{-5} cm^2/s for the proton diffusion constant in ice at -10 °C. This value fits nicely to the values of $D_H{}^+$ found in electrical conductivity measurements. It is plausible that a large fraction of protons with a large proton diffusion constant recombines with the RO^- already in the excited state. Thus, the experimental observation of the ground-state reaction is valid for the "slow" protons: the ones that were trapped in defects, impurities, etc.

The second set of reactions is based on a regular photoprotolytic cycle of a photoacid in neutral pH ice, i.e., in the absence of excess protons. The proton geminate recombination reaction of the proton with the $RO^{-}{}^*$ to reform the ROH* modifies the initial exponential decay of the ROH* to form the well-known complex nonexponential decay pattern.[52] The analysis of the ROH* decay profile provides a range of values for the proton diffusion constant: 3×10^{-5} to 1×10^{-4} cm^2/s.

The third set of experiments (to which this article belongs), concerns photoreactive molecules in ice that contains also a small concentration of mineral acid (a few mM). All three different kinds of probe molecules[39,57] in this kind of experiment indicated that $D_H{}^+$ is 10 times larger than in liquid water at 295 K.

In all experiments there is a proton reacting with a proton-reactive molecule. Two experiments (2 and 3) are measured within the electronically excited-state lifetime of the probe molecules, and are thus limited in their observation at long-time to about two radiative lifetimes, i.e., ~20 ns. Therefore, in order to observe the proton reaction, it should either be fast,

SCHEME 2

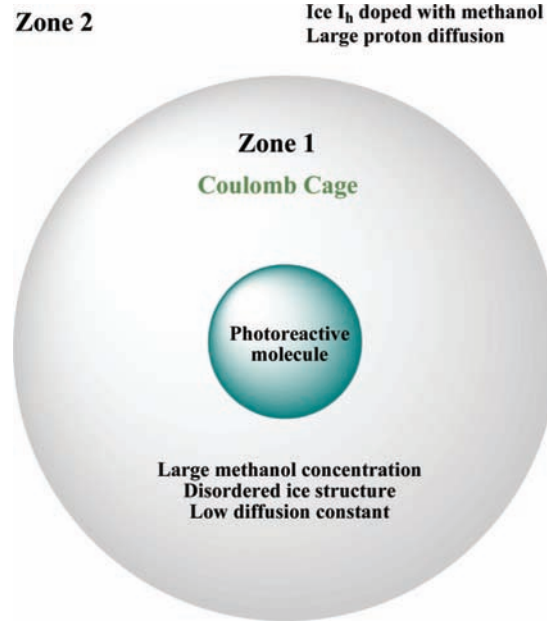

namely, its intrinsic reaction rate constant, k_a, and the diffusion-controlled rate constant, k_D, are large or the proton concentration should be high. In reactions of the first kind, the situation is reversed, so that the time resolution of the short times prevents us from watching the reaction dynamics at short times below 20 ns.

Scheme 2 may explain the large differences in $D_H{}^+$ as deduced from the three kinds of experiments described above. The photoreactive molecules create a large defect zone in the ice I_h structure. We designated it as zone 1 in the scheme. For a spherical symmetric case, zone 1 is a sphere of radius R. In this region, the proton diffusion constant is relatively small. Because of preferential solvation of the aromatic rings of the photoreactive molecules by methanol it contains more methanol molecules than the average concentration. The methanol serves as a cosolvent to aid the solvation of the large photoreactive molecules in the bulk ice. Methanol probably disrupts the ice structure, and also traps protons for a longer time than a water molecule, hence the smaller diffusion constant in zone 1. The proton geminate recombination is mostly experienced by the $RO^{-}{}^*$ within the Coulomb cage radius, R_D (see eq 6). R_D linearly depends on the charge, z, of the RO^- and inversely depends on the dielectric constant. The dielectric constant in ice has a high value of 100, for which the R_D of 2N68DS is ~17 Å, whereas for 1N4S ($z = -2$) R_D is ~12 Å. We estimate that the radius of zone 1 is ~25 Å, which is a length that can fit about 10 water molecules (the oxygen distance between adjacent water molecules in water and ice is about 2.75 Å). The proton geminate recombination process that determined $D_H{}^+$ is most effective at short distances from the photoacid RO^-. Protons beyond R_D are most likely to escape the recombination process. Experiments of the second kind thus exhibit a small value of $D_H{}^+$.

Zone 2 is the outer sphere, for which we assume that the ice structure is close to that of I_h ice. It includes Cl^-, H^+, methanol molecules, and orientational Bjerrum defects, D and L. For 1 mM of HCl, the average distance between H^+ is roughly 100 Å. Thus, for experiments of the third kind (excess protons in ice), in order for a proton to react with a photoreactive molecule, it must first diffuse over a long distance of ~100 Å. Only the last 30 Å or so are in zone 1, where the diffusion constant,

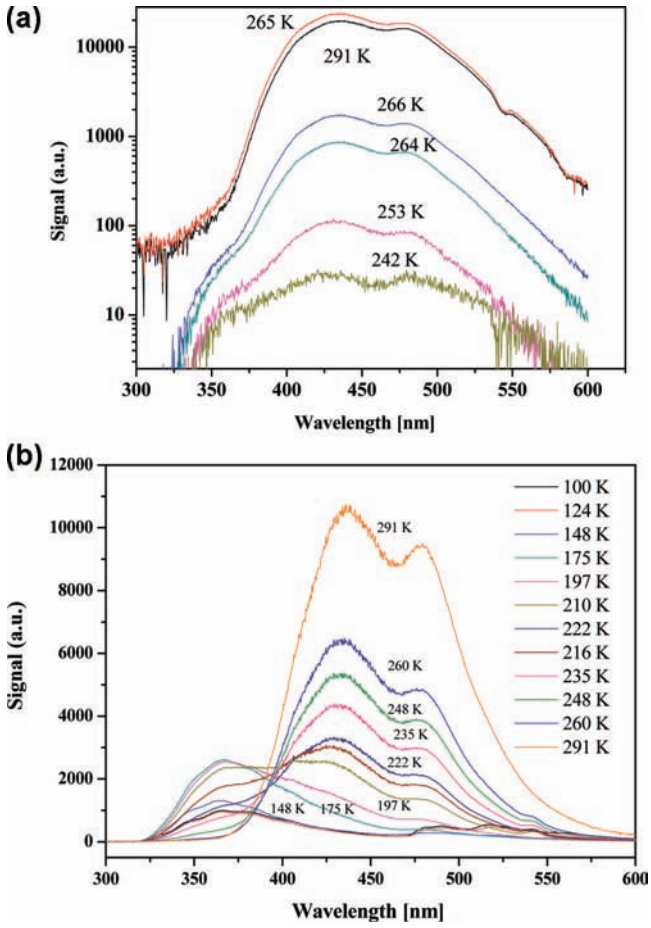

Figure 10. Steady-state emission of 1N4S in liquid and ice: (a) in pure water; (b) in 0.5% mole ratio methanol-doped ice.

D_{H^+}, is small. From the experimental results of the photoreaction in samples with excess protons we found that the proton diffusion constant in zone 2 is ~10 times larger than in zone 1.

Pure Water Ice and Ice of Low Methanol-Doping Levels. Figure 10a shows on a semilogarithmic scale the steady-state emission of 1N4S in neutral pH, pure liquid water and pure polycrystalline ice samples at various temperatures. While in the liquid state the intensity of the RO^- band at 440 nm is very large, in the ice phase the signal intensity drops by more than 2 orders of magnitude at temperatures below 245 K.

Figure 10b shows the steady-state emission of 1N4S in neutral pH methanol-doped liquid and ice (0.5% mole ratio of methanol) at various temperatures. A comparison between parts a and b of Figure 10 shows that in pure ice both the ROH and the RO^- bands decrease by more than a factor of 100, whereas the methanol-doped ice shows only a decrease by a factor of 2 of the ROH* and the RO^-* band intensities upon freezing (260 K).

A simple explanation to the large drop in the ROH and RO^- steady-state emission spectra intensity in pure ice sample is based on the findings of many studies regarding the poor solvation of ice. When a pure water sample freezes, the photoacid molecule is expelled from the bulk of the microcrystal and aggregates at the grain boundaries. The 1N4S, both as a dry powder and as an aggregate or a thin film at the grain boundaries of a polycrystalline ice at the ROH band, shows a large quenching rate, and the total fluorescence intensity is small and the decay is nonexponential with a short average decay time. Below 170 K the RO^- band intensity of the methanol-doped sample (Figure 10b) drops to less than 5% of the ROH band intensity. Thus, the rate of proton transfer is smaller than the ROH band nonradiative rate. At temperatures below 150 K a new emission band at wavelengths longer than 475 nm is observed. We attribute this band to phosphorescence.

Figure 11, a and b, shows the time-resolved emission of the ROH and the RO^- band of 1N4S respectively in pure water and ice samples (no methanol) as well as the signals in low methanol doping levels of 0.02% and 0.1% mole fraction. In neutral pH ice at temperatures below 260 K the time-integrated time-resolved emission signal of the RO^- band in pure H_2O samples decreases by a factor of 500 from the liquid sample signal, whereas for 0.1% mole fraction of methanol the signal decreased by a factor of 2. The decay profiles of the time-resolved emission signal measured at 450 nm (the RO^- band) of the neutral pH samples of pure ice and those doped with 0.02% mole fraction of methanol are nonexponential at temperatures below 265 K. The average decay time is calculated in the following manner: $\langle\tau\rangle^{-1} = \int_0^\infty f(t)\, dt$, where $f(t)$ is the normalized experimental time-resolved signal. The value of $\langle\tau\rangle$ of the signal measured at 450 nm in pure ice slightly depends on the temperature; the lower the temperature the smaller the $\langle\tau\rangle$. For 258 K, $\langle\tau\rangle = 1.71$ ns. The lifetime of the RO^- band of 1N4S in the liquid state is ~15 ns, and the decay is nearly a single exponential (see Figure 11b). For pure ice samples (no methanol), by comparing the time-integrated signal intensity (or the intensity of the steady-state spectra shown in Figure 10) and the average lifetime of the RO^- band in liquid and ice, while bearing in mind the limited time resolution of the TCSPC instrumentation (IRF of 35 ps), we estimate that about 97% of the molecules in ice do not fluoresce with a lifetime longer than ~20 ps. We explain this fact as a manifestation of the very small solubility of large molecules in pure ice. Most of the 1N4S molecules in a pure ice sample probably aggregate at the grain boundaries or are even pushed away from the bulk ice altogether and situated at the edge of the macroscopic sample. The steady-state emission of a dry solid powder of 1N4S shows a single band emission with a maximum at 360 nm. The spectrum is similar to the emission of the ROH band. The time-resolved emission of solid powder samples of 1N4S (no solvent) shows a weak signal with a peak at 360 nm of about 0.01 of that of a solution and a nonexponential decay with an average lifetime of about 40 ps similar to the one found for 1N4S in pure ice.[57] Upon dimerization and oligomerization of aromatic and heterocyclic compounds, the fluorescence intensity tends to drastically diminish. Thus, the pure ice sample's low emission intensity indicates that the 1N4S molecules are indeed excluded from the bulk ice and their position is either at the grain boundaries or even at the edge of the macroscopic sample. Similar nonfluorescent pure ice samples were also observed for 2N68DS and pyranine. The time-resolved emission of the RO^- band of 1N4S in 0.02% mole fraction of methanol shows intermediate properties between that of the pure water sample and the samples doped with 0.1% methanol or more. Another interesting point to note is that the time-resolved emission of the RO^- band of 1N4S in ice at 268 K seems to behave in between ice at temperatures lower than 263 K and liquid.

Low-Temperature Methanol-Doped Ice. Figure 12a shows the time-resolved emission of the ROH band of 1N4S in methanol-doped ice (0.5% mole ratio of methanol) with 4 mM of HCl measured at 360 nm at several temperatures below 240 K. The signals are nonexponential: the lower the temperature the longer the average decay time. Figure 12b shows the time-resolved emission of the same sample as in Figure 12a, except that here the signal is collected at the RO^- band at 450 nm. The RO^- band at temperatures above 170 K shows a signal

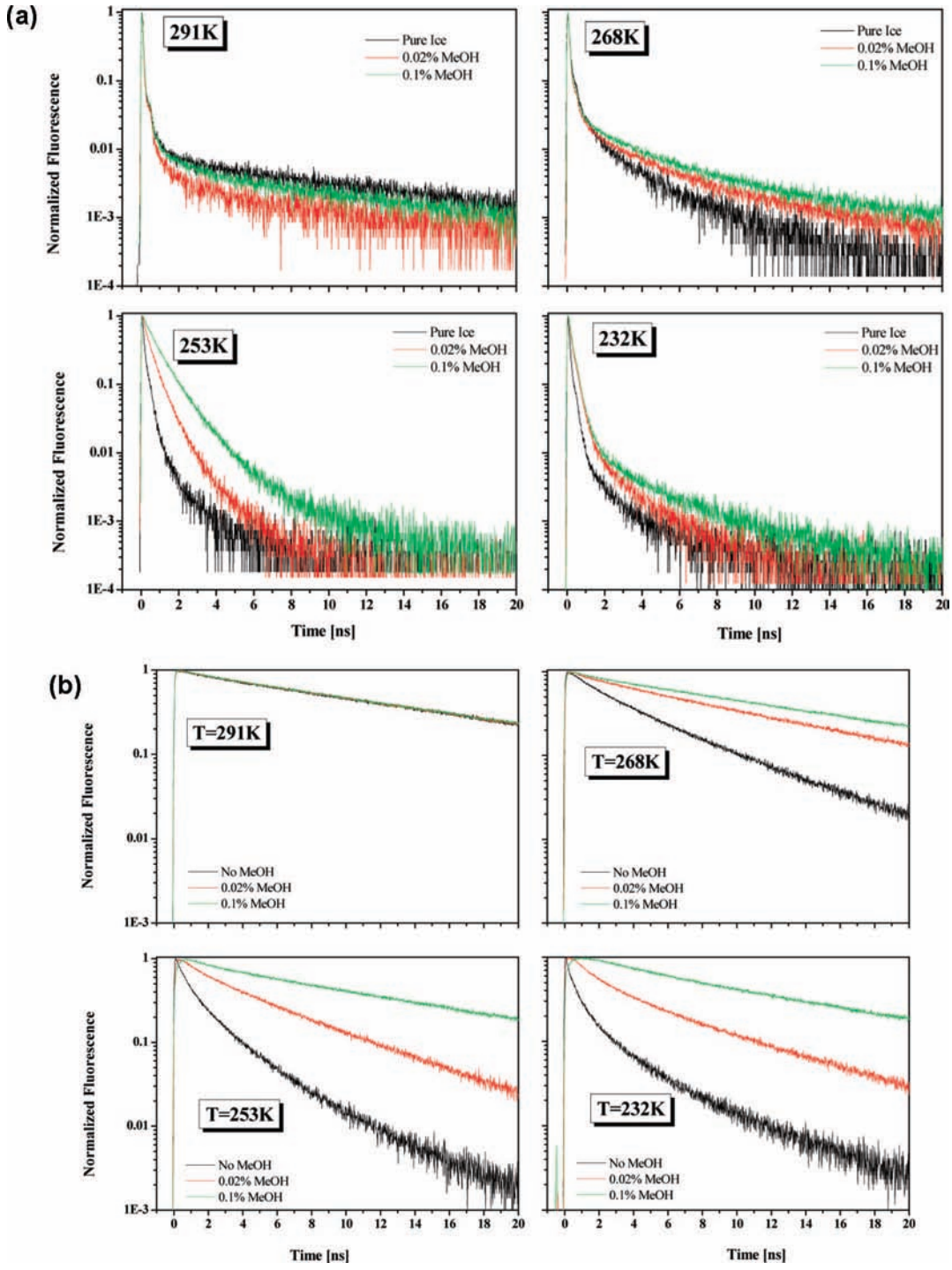

Figure 11. Time-resolved emission of 1N4S in pure ice, 0.02% methanol-doped ice and 0.1% methanol-doped ice: (a) ROH band measured at 360 nm; (b) the RO^- band measured at 450 nm.

buildup time that is determined by the decay of the ROH band. This is expected for a photoacid undergoing a photoprotolytic cycle, where the ground-state population is excited in its ROH form. Thus, the decay of the ROH and the rise of the RO^- signal in 4 mM HCl sample are determined by the transfer rate of the proton to the solvent. The decay of the RO^- signal depends on the temperature in the range of 173−237 K: the lower the temperature, the longer the decay time. The decay time of the RO^- band is determined by the radiative rate and the proton quenching reaction, $RO^{-}* + H^+ \rightarrow ROH$. The reaction rate constant at long times, k_∞, depends on both k_D and k_0. We attribute the temperature dependence of the decay rate of the RO^- to the temperature dependence of both k_0 and k_D. The latter depends on the proton diffusion constant, whose value strongly reduces with a decrease in temperature in this temperature range. Table 7 provides the values of k_0 and D_{H^+} at several temperatures in the range of 190−247 K. The RO^- signal at $T \geq 197$ K decays nearly exponentially. Below 197 K the RO^- signal decay is nonexponential. The steady-state emission, displayed in Figure 10b, shows that below 197 K the RO^- band intensity drops with a further decrease in the temperature, as does the intensity of the ROH band. The large nonexponential time-resolved emission signal of the RO^- band prevents us from accurately evaluating the proton diffusion constant at temperatures below 190 K.

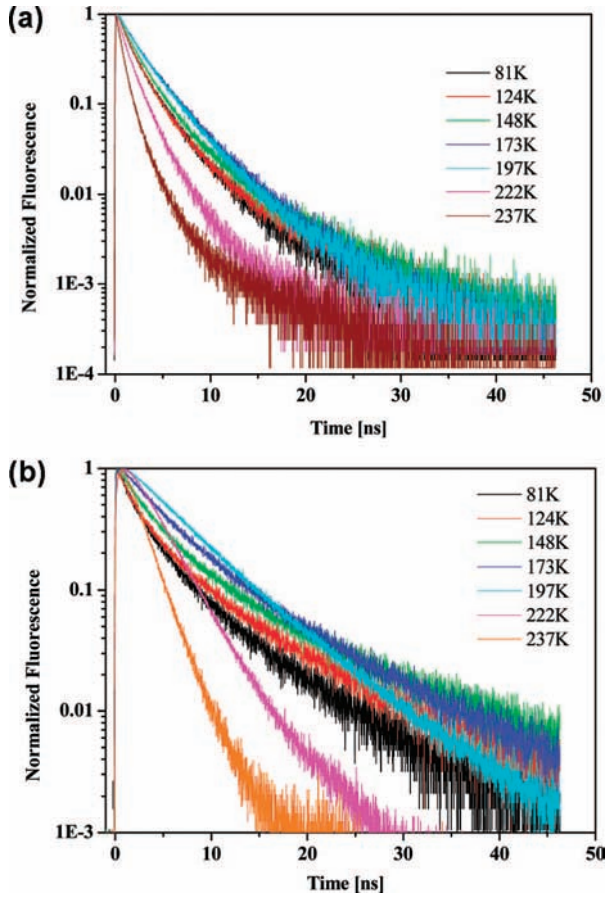

Figure 12. Low temperature time-resolved emission of 1N4S in 0.5% methanol-doped ice: (a) the ROH band measured at 360 nm; (b) the RO^- band measured at 450 nm.

TABLE 7: Low-Temperature Methanol-Doped Ice (0.5% mole ratio) with 4 mM of HCl[a]

phase	T (K)	k_0 (10^{11} s^{-1})	D (10^{-4} cm^2 s^{-1})	R_D (Å)
solid	197	1	0.45	14
solid	222	1.5	0.93	14
solid	237	2	2.6	14
solid	247	2.4	4.5	14

[a] The excited-state lifetime of 1N4S, $\tau = 14.7$ ns.

Ice Aging. Aging of ice samples may affect several properties of ice.[8] The following experiments show that within 7 h after the methanol-doped ice sample froze the time-resolved emission signals of both the ROH and the RO^- bands are time-independent. Figure 13a,b shows on a semilog scale the time-resolved emission signals of 1N4S in the ROH form measured at 360 nm and the RO^- form at 450 nm. Each figure contains six curves taken at different time lags after the initial freezing. The temperature of the ice sample was kept for 8 h in the temperature range of 220−260 K. The measurement of the TCSPC signal was taken at 253 ± 2 K. The methanol doping level of the sample was 0.5% mole ratio and the acid concentration was 4 mM.

As seen in Figure 13b the RO^- signals are almost identical along the 7 h of measurements. The ROH signals differ slightly and fluctuate between measurements. Except for the signal measured 60 min after the sample froze, all the signals decay in an almost identical pattern.

The main conclusion from these experiments is that the time-resolved emission of our samples are independent of the time elapsed from its initial freezing. This is true within a single

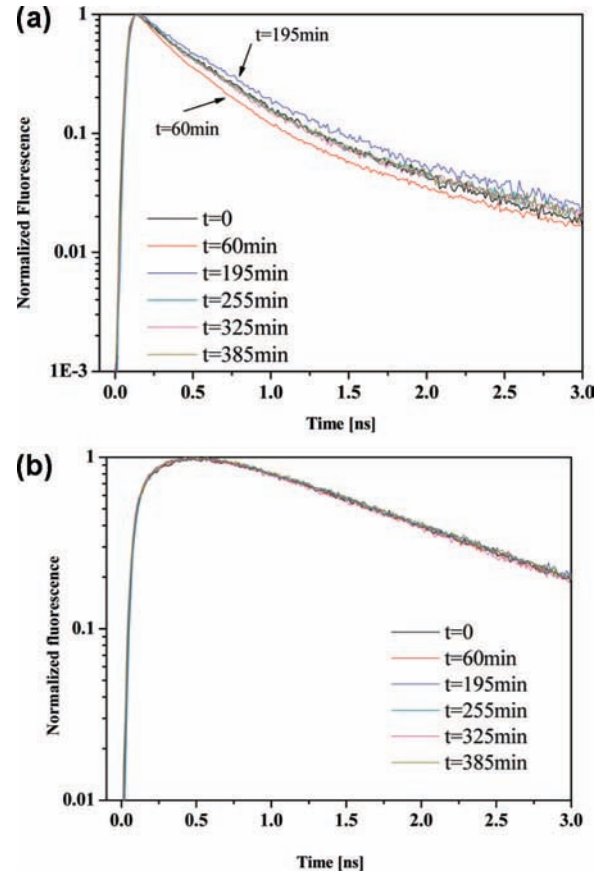

Figure 13. Long-term time-resolved emission of 1N4S in ice during a 7 h period: (a) the ROH band at 360 nm; (b) the RO^- band at 450 nm.

day's working hours, i.e., about 8 h. Since we were unable to see a time vectorial change in the TCSPC of both ROH and RO^- within 7 h (Figure 13, a and b) it is reasonable to assume that even within times longer by a factor of 5 the signal will not change by much. It is also important to note that during the many months of research on 1N4S in ice and years with other compounds[39] the TCSPC results of a particular sample were invariant under a change of the date, in which the measurements were taken. The results are also insensitive to the sample preparation method, the cooling rate and the freezing procedure.

Connection between the Determination of the Diffusion Constant and the Dielectric Properties of Ice. Equations 4−6 show that the proton recombination rate strongly depends on the dielectric constant. The large acid effect in ice may be the outcome of a large drop in the value of the dielectric constant as a consequence of doping the ice with HCl, rather than of a large diffusion constant as proposed in the present study. If the dielectric constant decreases with temperature in the presence of HCl, then the diffusion-controlled rate constant will be strongly affected. The Debye radius R_D scales inversely with the dielectric constant $R_D = ze^2/\varepsilon_s k_B T$ (eq 4). The second-order diffusion-controlled rate constant depends on R_D, i.e., $k_D \cong 4\pi N' D_{H^+} R_D/(1 - \exp(-R_D/a))$. The large increase in the fluorescence quenching of the RO^- of 1N4S in ice arises not only because of a large increase in D_{H+}, but partially also because of the large increase of R_D, since the dielectric constant of HCl-doped ice according to the theory below is smaller than water, i.e., $\varepsilon = 78$.

The conductivity of the ion defects is given by $\sigma_\pm = \sum_{i=1}^{2} n_i \mu_i |e_i|$, where n is the ion defect number density, $|e_i|$ is the ion effective charge, and μ is the mobility that scales linearly with

the diffusion constant by the Stokes−Einstein relation, $\mu = D \cdot e/k_B$. It was previously reported that the dielectric constant of ice strongly decreases with an HF acid concentration.[57] Based on Jaccard's theory,[11] which links the defect conductivity with the dielectric constant, and on Hubmann's corrections[58] the static dielectric constant ε_s is given by

$$\varepsilon_s - \varepsilon_\infty = \frac{1}{\varepsilon_0 \Phi} \frac{\left(\frac{\sigma_\pm}{e_\pm} - \frac{\sigma_{DL}}{e_{DL}}\right)^2}{\left(\frac{\sigma_\pm}{e_\pm^2} + \frac{\sigma_{DL}}{e_{DL}^2}\right)^2} \tag{7}$$

where σ_{DL} are the conductivity of the Bjerrum defects. $e_\pm^2$ and e_{DL}^2 are the effective electrical charges of the ionic and Bjerrum defects, respectively, and Φ is the product of a geometrical factor and the thermal energy $k_B T$. ε_s strongly depends on the density of the two types of defects.

If $\sigma_{DL} \gg \sigma_\pm$, as is the case for pure ice, where $n_{DL} \approx 10^{13}$ cm^{-3} and $n_\pm = 10^7$ cm^{-3}, then

$$\varepsilon_s - \varepsilon_\infty = \frac{\sqrt{3}}{9\varepsilon_0 r_{00} k_B T} \left(\frac{2qb}{r_{00}}\right)^2 \tag{8}$$

whereas if $\sigma_\pm \gg \sigma_{DL}$ (ice doped with HCl, $n_\pm > 10^{13}$ cm^{-3}), then

$$\varepsilon_s - \varepsilon_\infty = \frac{3\sqrt{3}}{32\varepsilon_0 r_{00} k_B T} \left(\frac{pa}{r_{00}}\right)^2 \tag{9}$$

If $\sigma_\pm \cong \sigma_{DL}$ then $\varepsilon_s \cong \varepsilon_\infty$.

The quantities $2qb/r_{00}$ and pa/r_{00} are approximately the effective charges e_{DL} and $e_\pm$, respectively.

HCl is a very strong acid, and therefore we assume that all the HCl molecules dissociated in the small concentration range we explored ($0.25 < c \leq 4$ mM), so that $\sigma_\pm \gg \sigma_{DL}$. According to Hubmann's expression, which is derived from Jaccard's theory, ε_s is expected to be ∼44 in the HCl doping level of our experiments. In the original expression of Jaccard's theory when $\sigma_\pm \gg \sigma_{DL}$, $\varepsilon_s = 22$.

Takei and Maeno[55,56] studied the electrical conductivity and the dielectric properties of HCl doped ice in single crystals grown from HCl liquid solutions of 4×10^{-6} to 1×10^{-4} M HCl. The concentration of HCl incorporated in the ice is rather small, although not directly measurable. Thibert and Dominé[59] found that HCl gas is immiscible in large single crystal ice as well. The ion conductivity $\sigma_\pm$ of all samples in Takei and Maeno's study[55,56] is almost temperature independent in the range of $230 < T < 270$ K. As in Takei and Maeno's experiments we also found that the proton diffusion constant is almost temperature independent (within a factor of 2) in the range of 235−260 K. At lower temperatures, the $\sigma_\pm$ conductivity decreases with a relatively large activation energy of 0.31 eV.[56]

The study of Steinemann[57] showed that the dielectric constant of HF-doped ice strongly depends on the acid concentration. However, in our experiments the value of the proton diffusion constant extracted from the fit of the experimental results by using the diffusion-assisted kinetic model is independent of the proton concentration in the range of $0.25 < c < 4$ mM. This and previous findings[39] suggest that the effective dielectric constant in the acid-doped ice studied in our work was nearly constant at all acid concentrations used, i.e., $0.25 < c < 5$ mM. In the extreme case, where the dielectric constant decreases to $\varepsilon_s = 44$ according to eq 9 and $k_D \cong 4\pi N' D_{H^+} R_D$, R_D is assumed to almost double. On the other hand, the value of the proton diffusion constant, which we derived from the experimental time-resolved emission data, is supposed to be half of the value we deduced for $\varepsilon_s = 100$. In that case, and assuming that $\varepsilon_s = 44$, proton diffusion in ice should only be 5 times larger than in water at 295 K, rather than 10 times, or about 15 times larger than in supercooled liquid at ∼265 K.

Proton Reaction at Grain Boundaries and Characterization of the Ice Sample. The second possible explanation for the large acid effect on the quenching rate of the RO^- of 1N4S and 1N3S in doped ice is along the lines of other observations,[6] suggesting that dopants tend to be excluded from the ice bulk and aggregate on grain boundaries. If that is the case, rather than being incorporated in the bulk of an ice microcrystal, the photoacid molecules in our experiments are positioned at the grain boundaries. Consequently, the proton fluorescence quenching reaction with the RO^{*-} takes place at the grain boundaries and not in the bulk.

There are two possibilities for the proton quenching of the RO^{-}*: (a) both the protons and the photoacids are at the grain boundaries; (b) the protons are in the bulk, while the photoacid is at the grain boundaries. We shall first discuss the second possibility and assume that the protons stay in the bulk. It is well-known and documented that single-crystal ice conductivity increases when the ice is doped with acids and bases.[8−10,55,56] Therefore, at least a significant fraction of protons are distributed in the bulk of large single crystals. The naphthol molecules themselves are at the grain boundaries, as are the counterions (sodium ions from the sulfonate salt and chlorides from the HCl). Thus, the 1-naphthol derivatives concentration is very large at the surface, whereas the excess proton concentration is small. Proton fluorescence quenching takes place at the surface of the polycrystalline ice. The experimental results are then indicative of proton diffusion from the bulk toward the grain boundaries. The main difference between this description and the pure bulk reaction we adopted in our previous studies[60] using 2N68DS and FMN and implemented also in the present work is the dimensionality of the problem. The proton diffuses with a three-dimensional bulk diffusion constant toward a nearby surface and reacts with the molecules at the grain boundaries. The proper description of the diffusion toward the surface may be regarded as one-dimensional since the excitation laser spot diameter is rather wide (500 μm). The main conclusion of this study and of the previous ones that the proton diffusion in bulk ice is 10 times larger than in water qualitatively applies also in the case discussed above.

When both the proton and the RO^{-}* are on the surface of the ice microcrystals, proton diffusion happens on the surface, and the surface concentration of both the proton and the RO^{-}* is large. The expected reaction rate is supposedly large, since it linearly depends on the proton concentration. Qualitatively, the experimental results indeed show a 10-fold increase in the overall reaction rate compared to liquid water. If we assume that the microcrystal size is 10 μm and use both the values of the diffusion constant in water, $k_D \cong 5 \times 10^{10}$ M^{-1} s^{-1}, and the large effective proton concentration on the surface of the grain boundaries, then the fluorescence quenching actually measured is smaller by a factor of 10 than the calculated reaction rate. Thus, in the case described above, where both the protons and the acid are at the grain boundaries, the calculated diffusion-controlled reaction rate should be smaller than $k_D \cong 5 \times 10^{10}$

M^{-1} s^{-1}, the value for protons in water at 298 K, and the deduced surface proton diffusion constant maintains $D_{H^+}^{sur} < D_{H^+}^{liq}$.

In a recent paper[60] we characterized the position of a photoacid in methanol-doped ice polycrystalline samples by employing Förster's electronic energy transfer (EET) process between two chromophores. We used the EET process to estimate the average distance between two large aromatic compounds in methanol-doped polycrystalline ice samples. In order to demonstrate how the strength and sensitivity of the EET method determine where the dopants are positioned in the ice samples, we calculated the average distance between the positions of both donor and acceptor molecules for two particular cases. For a 10 μm cubic crystal with a bulk concentration of 1 mM, the average distance between adjacent photoacid molecules at the grain boundaries is assumed to be equivalent to about 5 Å. However, in bulk ice the distance between a donor and an acceptor is supposedly more than 20 times larger, i.e., ~100 Å. In the case of an average distance of 5 Å the EET process is very efficient and the donor decay time is a few picoseconds. The actual donor decay measured in the experiments of our previous study[60] was close to its radiative rate $\tau = 12$ ns. Förster's EET experiments indicate that in methanol-doped ice the photoacid molecules tend to stay in the bulk of the microcrystal rather than aggregate at the grain boundaries upon freezing of the sample. We used 2N68DS in its deprotonated form, RO^-*, as the EET donor, and fluorescein disodium salt (uranine) as the acceptor. We compared the experimental results of the time-resolved EET emission of samples in an aqueous liquid state with the results in ice. The EET process at an acceptor concentration range of $0.2 < c < 1$ mM showed a small, but similar, energy transfer rate for both liquid and ice samples (the critical radius being $R_0 = 56$ Å). From the EET experimental results we conclude that 2N68DS tends to stay in the polycrystalline ice bulk. For a concentration of 1 mM mineral acid, the average distance between an excess proton and a RO^-* is also 5 Å, which is about 2 water molecules. The equivalent bulk concentration is a few molars. If we assume a modest diffusion-controlled reaction rate constant of $k_D \sim 5 \times 10^{10}$ M^{-1} s^{-1}(proton diffusion in water), then the reaction will probably take place within 20 ps or less. In the current study we also measured the EET rate between the RO^-* of 1N4S (the donor) and uranine (the acceptor). At 268 K, the EET rate in ice is comparable to that in the liquid state. These results are in favor of the first description in this article and the previous studies,[39] where we assumed that both the excess protons and the photoacid molecules are homogeneously distributed in the bulk of the ice microcrystal. These results supported the first description of this article and the previous studies,[39] where we assume that both the excess protons and the photoacid molecules are homogeneously distributed in the bulk ice microcrystal.

Summary

We studied the fluorescence quenching of the RO^-* of 1-naphtholsulfonate derivatives in liquid water and in ice in the presence of small concentrations of the strong mineral acid HCl. We used a time-resolved emission technique to monitor the excess fluorescence quenching by excess protons in both liquid water and in ice. The electrical conductivity measurements of Eigen[4] in the early 1960s resulted in a surprisingly large mobility value for the proton in ice. The results of the present study and of our previous one[39] indicate that the proton mobility in ice is indeed larger than in water, at least on a nanometric distance scale. Already in 1983 Nagle[48] advocated the existence of proton wires in ice and in enzymatic systems in which the proton transport is carried out via a concerted mechanism (Grotthuss mechanism) on a limited length scale. Under certain assumptions and approximations, we deduced the proton diffusion constant in bulk ice from the experimental data fit by using the irreversible diffusion-assisted recombination model based on the Debye-Smoluchowski equation. We found that the proton diffusion in ice I_h at 240−260 K is about 10 times larger than in liquid water at 295 K. This large proton diffusion is in accord with our more recent studies,[39] where we used the 2-naphthol-6,8-disulfonate (2N68DS) photoacid and flavin mononucleotide as probes for the diffusion constant of protons in ice. Ice conductance has been extensively studied for more than four decades. Our findings are in accord with the electrical measurements of Eigen and deMaeyer,[40,41] but contradict conductivity measurements of ice from 1968 to this day. We explained the large difference between the results of the present study and the conductivity measurements by the proton diffusion length in the two types of measurements. In our measurements, we monitored a small diffusion sphere of about 50 nm around the excited photoacid molecules, whereas in the conductance measurements the distances between electrodes were in the range of 1 mm.

Acknowledgment. We thank Professor I. Goldberg for the X-ray diffraction measurement. This work was supported by grants from the Israel Science Foundation and the James-Franck German-Israel Program in Laser-Matter Interaction.

Supporting Information Available: An X-ray diffraction pattern of methanol-doped ice (0.5% mole ratio) measured at 245 K. This information is available free of charge via the Internet at http://pubs.acs.org.

References and Notes

(1) Bell, R. P. *The Proton in Chemistry*, 2nd ed.; Chapman and Hall: London, 1973.
(2) *Proton Transfer Reaction*; Caldin, E. F., Gold, V., Eds.; Chapman and Hall: London, 1975.
(3) (a) Weller, A. *Prog. React. Kinet.* **1961**, *1*, 189. (b) , *Z. Phys. Chem. N. F.* **1958**, *17*, 224.
(4) (a) Eigen, M. *Angew. Chem., Int. Ed.* **1964**, *3*, 1. (b) Eigen, M.; Kruse, W.; Maass, G.; De Maeyer, L. *Prog. React. Kinet.* **1964**, *2*, 285.
(5) Uras-Aytemiz, N.; Joyce, C.; Devlin, J. P. *J. Phys. Chem. A* **2001**, *105*, 10497.
(6) Devlin, J. P.; Gulluru, D. B.; Buch, V. *J. Phys. Chem. B* **2005**, *109*, 3392.
(7) Fletcher, N. H. *The Chemical Physics of Ice*; Cambridge University Press: London, **1970**.
(8) Hobbs, P. V. *Ice Physics*; Clarendon Press: Oxford, UK, 1974; Chapter 2.
(9) Von Hippel, A.; Runck, A. H.; Westphal, W. B. *Physics and Chemistry of Ice*, 5th ed.; Walley, E., Jones, S. J., Gold, L. W., Eds.; Royal Society of Canada: Ottawa, 1973; p 236.
(10) Petrenko, V. F.; Whitworth, R. W. *The Physics of Ice*; Oxford University Press: Oxford, UK, 1999.
(11) Jaccard, C. *Ann. N.Y. Acad. Sci.* **1965**, *125*, 390–400.
(12) Bjerrum, N. *Science* **1952**, *115*, 385.
(13) Kobayashi, C.; Saito, S.; Ohmine, I. *J. Chem. Phys.* **2001**, *115*, 4742.
(14) Podeszwa, R.; Buch, V. *Phys. Rev. Lett.* **1999**, *83*, 4570.
(15) Eigen, M.; de Maeyer, L. In *The Structure of Electrolytic Solutions*; Wiley: New York, 1959; p 64.
(16) Kelly, I. J.; Salomon, R. R. *J. Phys. Chem.* **1969**, *50*, 75.
(17) Camplin, G. C.; Glen, J. W. *Physics and Chemistry of Ice*, 5th ed.; Walley, E., Jones, S. J., Gold, L. W., Eds.; Royal Society of Canada: Ottawa, 1973; p 256.
(18) Kunst, M.; Warman, J. M. *J. Phys. Chem.* **1983**, *87*, 4093.
(19) Wooldridge, P. J.; Devlin, J. P. *J. Chem. Phys.* **1988**, *88*, 3086.
(20) Fisher, M.; Devlin, J. P. *J. Phys. Chem.* **1995**, *99*, 11584.
(21) Everest, M. A.; Pursell, C. J. *J. Chem. Phys.* **2001**, *115*, 9843.
(22) Geil, B.; Kirschgen, T. M.; Fujara, F. *Phys. Rev. B: Condens. Matter Mater. Phys.* **2005**, *72*, 014304.

(23) Kang, H. *Acc. Chem. Res.* **2005**, *38*, 893.
(24) Moon, E.; Lee, C.; Kang, H. *Phys. Chem. Chem. Phys.* **2008**, *10*, 4814.
(25) Cowin, J. P.; Tsekouras, A. A.; Iedema, M. J.; Wu, K.; Ellison, G. B. *Nature* **1999**, *398*, 405.
(26) Stoner-Ma, D.; Melief, E. H.; Nappa, J.; Ronayne, K. L.; Tonge, P. J.; Meech, S. R. *J. Phys. Chem. B* **2006**, *110*, 22009.
(27) van Thor, J. J.; Zanetti, G.; Ronayne, K. L.; Towrie, M. *J. Phys. Chem. B* **2005**, *109*, 16099.
(28) Vendrell, O.; Gelabert, R.; Moreno, M.; Lluch, M. *J. Phys. Chem. B* **2008**, *112*, 5500.
(29) Ireland, J. E.; Wyatt, P. A. *Adv. Phys. Org. Chem.* **1976**, *12*, 131.
(30) (a) Gutman, M.; Nachliel, E. *Biochim. Biophys. Acta* **1990**, *391*, 1015. (b) Pines, E.; Huppert, D. *J. Phys. Chem.* **1983**, *87*, 4471.
(31) Tolbert, L. M.; Solntsev, K. M. *Acc. Chem. Res.* **2002**, *35*, 19.
(32) (a) Rini, M.; Magnes, B. Z.; Pines, E.; Nibbering, E.T. J. *Science* **2003**, *301*, 349. (b) Mohammed, O. F.; Pines, D.; Dreyer, J.; Pines, E.; Nibbering, E. T. J. *Science* **2005**, *310*, 5745.
(33) Tran-Thi, T. H.; Gustavsson, T.; Prayer, C.; Pommeret, S.; Hynes, J. T. *Chem. Phys. Lett.* **2000**, *329*, 421.
(34) Agmon, N. *J. Phys. Chem. A* **2005**, *109*, 13.
(35) Spry, D. B.; Fayer, M. D. *J. Chem. Phys.* **2008**, *128*, 084508.
(36) Siwick, B. J.; Cox, M. J.; Bakker, H. J. *J. Phys. Chem B* **2008**, *112*, 378.
(37) Buch, V.; Milet, A.; Vácha, R.; Jungwirth, P.; Devlin, P. *PNAS* **2007**, *104*, 7342.
(38) Mondal, S. K.; Sahu, K.; Sen, P.; Roy, D.; Ghosh, S.; Bhattacharyya, K. *Chem. Phys. Lett.* **2005**, *412*, 228.
(39) (a) Uritski, A.; Presiado, I.; Huppert, D. *J. Phys. Chem. C* **2008**, *112*, 11991. (b) Uritski, A.; Presiado, I.; Huppert, D. *J. Phys. Chem. C* **2008**, *112*, 18189.
(40) Eigen, M.; deMayer, L.; Spatz, H. *Ber. Bunsenges. Phys. Chem.* **1964**, *68*, 19.
(41) Eigen, M.; deMayer, L. *Proc. R. Soc. London* **1958**, *247*, 505.
(42) Cohen, B.; Huppert, D.; Agmon, N. *J. Phys. Chem A* **2001**, *105*, 7165.
(43) Von Smoluchowski, M. *Z. Phys. Chem.* **1917**, *92*, 129.
(44) Tachiya, M. *Radiat. Phys. Chem.* **1983**, *21*, 167.
(45) Szabo, A. *J. Phys. Chem.* **1989**, *93*, 6929.
(46) Agmon, N.; Szabo, A. *J. Chem. Phys.* **1990**, *92*, 5270–5284.
(47) Krissinel, E. B.; Agmon, N. *J. Comput. Chem.* **1996**, *17*, 1085.
(48) Nagle, J. F. *J. Phys. Chem.* **1983**, *87*, 4086.
(49) Lee, C. W.; Lee, P.-R.; Kang, H. *J. Chem. Phys.* **2007**, *127*, 84701.
(50) Park, S.-C.; Jung, K.-H.; Kang, H. *J. Chem. Phys.* **2004**, *121*, 2765.
(51) Pines, E.; Huppert, D. *Chem. Phys. Lett.* **1985**, *116*, 295.
(52) Pines, E.; Huppert, D.; Agmon, N. *J. Chem. Phys.* **1988**, *88*, 5620–5630.
(53) Agmon, N.; Pines, E.; Huppert, D. *J. Chem. Phys.* **1988**, *88*, 5631–5638.
(54) Devlin, J. P. *J. Chem. Phys.* **1988**, *89*, 5967.
(55) Takei, I.; Maeno, N. *J. Phys. Chem.* **1984**, *81*, 6186.
(56) Takei, I.; Maeno, N. *J. Phys. (Paris)* **1987**, *48*, 121 (Colloque C1).
(57) Steinemann, S. *Helve. Phys. Acta* **1957**, *30*, 581.
(58) Hubmann, M. *Z. Phys. B* **1979**, *32*, 127.
(59) Thibert, E.; Dominé, F. *J. Phys. Chem. B* **1997**, *101*, 3554.
(60) Uritski, A.; Huppert, D. *J. Phys. Chem. A* **2008**, *112*, 3066.

JP806242A